Removal of total ammoniacal nitrogen from reject water through selective electrodialysis reversal and bipolar electrodialysis

Kaniadakis, Iosif; van Lier, Jules B.; Spanjers, Henri

Removal of total ammoniacal nitrogen from reject water through selective electrodialysis reversal and bipolar electrodialysis

Iosif Kaniadakis [*], Jules B. van Lier, Henri Spanjers

Delft University of Technology, Faculty of Civil Engineering and Geosciences, Stevinweg 1, 2628 CN Delft, The Netherlands

ARTICLE INFO

ABSTRACT

The removal of ammonium and ammonia, represented as total ammoniacal nitrogen (TAN), from reject water through electro-dialysis (ED) and bipolar membrane electrodialysis (BPMED) encounters challenges such as organic fouling, NH_3 back-diffusion, and high energy consumption. The efficacy of electrodialysis reversal (EDR) combined with bipolar membrane electrodialysis using cation-exchange membranes (BPC) was assessed as a more practical configuration (EDR + BPC). Additionally, a novel configuration involving monovalent selective cation-exchange membranes (MSCEMs) in an EDR + BPC setup (SEDR + BPC) was investigated. Comparisons were made among BPMED, EDR + BPC, and SEDR + BPC under three load ratios (L_N) of 0.8, 1, and 1.3 during continuous operation. The innovative SEDR + BPC configuration, with an L_N of 0.8, exhibited the lowest energy consumption for transported TAN (E_{TAN}) at 4.4 MJ·kgN^{-1} removal and achieved the highest TAN removal efficiency of 78 % with an L_N of 1.3. In contrast to conventional BPMED, SEDR + BPC allowed for the recovery of potentially back-diffused NH_3 into the acid chamber, minimizing transport losses. Furthermore, scaling in the base chamber was reduced due to the contribution of MSCEMs when applying an L_N of 0.8. The MSCEMs increased the molar ratio of TAN over ($Mg^{2+} + Ca^{2+}$) in the concentrate and decreased it in the diluate. EDR + BPC and SEDR + BPC configurations exhibited stable and lower cell resistance throughout the operation compared to BPMED, attributed to their ability to generate higher concentration gradients. The results clearly demonstrated the feasibility of low-energy TAN removal from real reject water from sludge anaerobic digestion using the SEDR + BPC setup.

1. Introduction

Total ammoniacal nitrogen (TAN) surplus in soil and aqueous environment is a major environmental concern due to the excessive accumulation of reactive nitrogen in soil and aqueous ecosystems [1–3]. Specifically, TAN in the form of NH_4^+ and NH_3 (dissolved or gas) is one such form of nitrogen that has been identified as a key contributor to nitrogen pollution [4]. In wastewater treatment plants (WWTPs), TAN is also found in high concentrations (>0.5 g·L^{-1}) in residual streams such as reject water from anaerobic digestion (AD) of sludge [5]. A growing interest during the last two decades has generated a wide development on electrochemical removal of TAN and subsequent recovery as NH_3.

Consequently, the potential of NH_3 to provide valuable products or even generate electrical energy through SOFC combustion raised the interest for recovery of TAN from side-streams such as reject water from anaerobic digestion (AD) [6,7].

1.1. Bipolar membrane electrodialysis (BPMED) for TAN-removal and recovery from residual streams

In recent research, the removal and recovery of TAN electrochemically has been widely discussed introducing the efficacy of BPMED for such case. BPMED has been successfully applied in the recovery of NH₄-OH from animal manure [8] and urine [9–11]. Other studies have

Fig. 1. Schematic representation of the membrane configuration in the used conventional BPMED stack. The reject water is introduced into the diluate chamber, and the applied current initiates the transport of cations, including TAN, towards the base chamber while anions, represented by negatively charged organic matter, are transported to the acid chamber. Simultaneously, the BPM facilitates the water splitting, resulting in the generation of H^+ and OH^- ions. Due to their respective charges, the H^+ ions are directed towards the acid compartment, contributing to the formation of an acidic solution, while the OH^- ions migrate towards the base chamber, leading to the formation of a base solution.

successfully recovered TAN into an NH_4-OH solution from synthetic and real AD reject water of sludge dewatering by including BPMED and ED in the process [9,12–14].

In BPMED, the bipolar membrane (BPM) enables the dissociation of water into H^+ and OH^- ions for the production of acidic and base streams, respectively. A BPMED-stack is typically comprised of an anion-exchange membrane (AEM), a cation-exchange membrane (CEM) and the BPM. TAN present in the feed solution will be transported and concentrated into the base stream and combined with OH^- to form dissolved NH_4-OH [15]. Therefore, as depicted in Fig. 1, the potentially polluting TAN is removed from the water stream and subsequently recovered in the form of NH_3 as a more valuable product. However, during these treatments BPMED frequently encounters challenges when treating TAN-loaded streams, which can be attributed to two factors: i) a low concentration gradient of TAN between the feed and the concentrate, as reported in several studies [11–13], and ii) competitive transport between NH_4^+ and divalent cations (Ca^{2+}, Mg^{2+}), with the latter also causing inorganic scaling on the CEM surface, as has been observed previously [11–13]. Scaling is the result of alkaline conditions in the base solution due to the presence of OH^- and the saturated concentrations of divalent cations leading to precipitation. Furthermore, the recovered NH_3 can potentially diffuse from the base to the acid solution as clearly demonstrated by van Linden et al. [14] and considered a loss.

1.2. Challenges of electrodialysis (ED) and BPMED on NH_3 recovery from real side-streams

Conventional ED has emerged as a promising technology for the concentration of nutrients from various wastewater streams. Specifically, ED can provide high TAN-concentrated streams from side-streams such as, sludge reject waters from AD processes [26], swine manure [27,28], and domestic wastewater [29].

The main advantage of ED compared to a three-compartment BPMED

is the potential in removing TAN from wastewater streams by generating a TAN-concentrated solution at lower energy consumption (E_{TAN}). In a recent study conducted by van Linden et al. [16], ED removed up to 90 % of TAN and reached a concentration factor of 6.7 from a synthetic solution representing sludge reject water with a final E_{TAN} of 5 MJ kgN^{-1}. Moreover, ED was evaluated at a pilot scale on real AD reject water, resulting in a highly concentrated solution with a concentration factor of 8.3, a current efficiency of 79 %, and an overall E_{TAN} of 17.6 MJ kgN^{-1} [17]. However, the operation of ED for such an application, comes with challenges such as organic membrane fouling [15] or colloidal fouling of the AEM [18]. Consequently, the resulting membrane fouling contributes to a higher E_{TAN}, due to an increase in overall membrane resistance [12].

Overall, fouling poses a formidable challenge to sustained operational efficiency in ED. However, the intrinsic symmetrical membrane arrangement of ED configurations presents a unique opportunity for applying reversed polarity as a fouling mitigation strategy. Electrodialysis reversal (EDR) stands out as a promising approach, harnessing controlled reversed polarity to combat organic and colloidal fouling. By periodically reversing polarity, EDR facilitates the detachment of fouling matter from membrane surfaces, thus restoring the performance [19].

1.3. Strategies for improving the process

In order to cope with low concentration gradients and inorganic scaling, pre-treatment technologies have been introduced in the past. Struvite reactors have being recently applied as pre-treatment to reduce the concentration of divalent cations such as Mg^{2+} and Ca^{2+}, in the feeding stream [17,20]. However, in residual side-streams such as sludge reject water, the molar concentration of TAN by far exceeds that of phosphate resulting in a limited removal efficiency (15–30 %) of TAN through struvite formation [21,22].

Donnan dialysis has been utilized in previous studies as a pre-
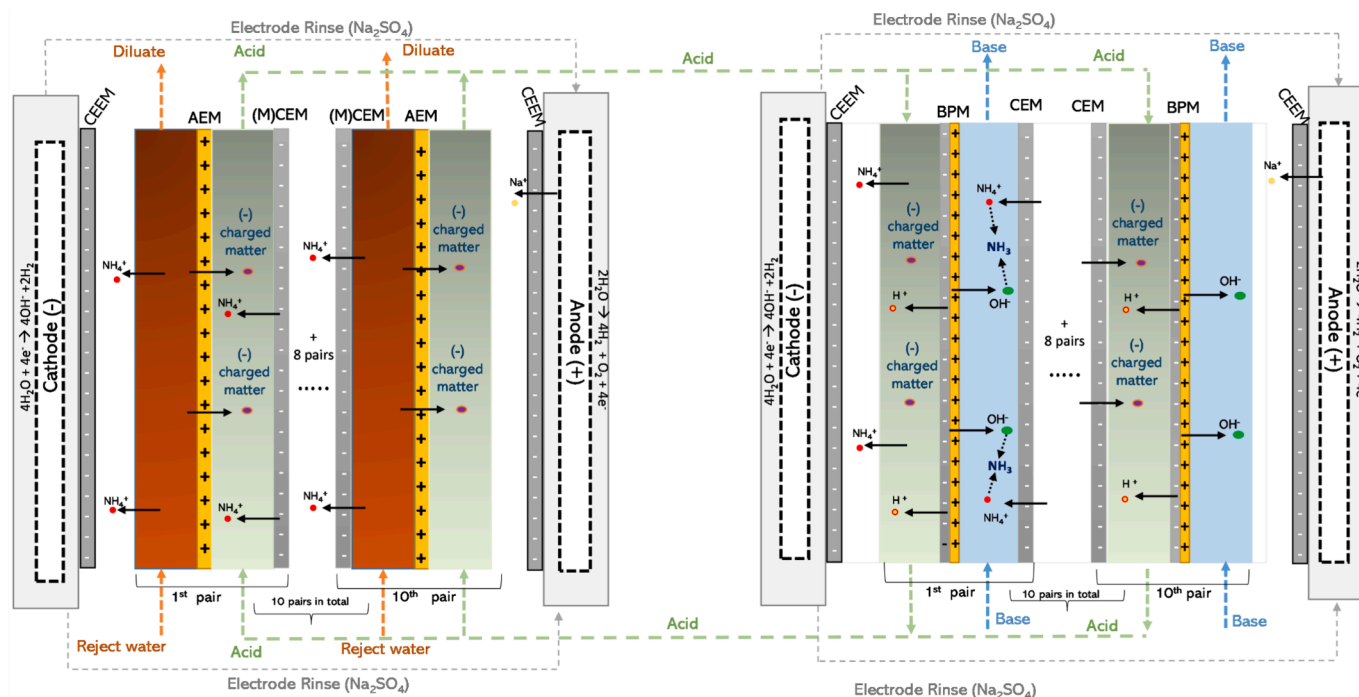
Fig. 2. Schematic representation of the used combination of ED and BPC. Left unit represents the ED concept, which involves a pair of membranes consisting of an AEM and a CEM for EDR. When the stack was operated as SEDR, the CEM was replaced with an MSCEM. The reject water is introduced into the diluate chamber, and as the process progresses, cations such as TAN and negatively charged matter are transported into the acid chamber. The acid chamber becomes at the same time the concentrate for the EDR and the feed for BPC. Within the base chamber, the concentrated TAN reacts with OH^- generated by the BPM, resulting in the formation of NH_3.

treatment method for ED and BPMED systems for the removal of Ca^{2+} and Mg^{2+} ions [12,13]. However, for an efficient application of Donnan dialysis, the liquid stream needs to be acidified to low pH levels (2–4) to guarantee an ionic form of TAN as NH_4^+ for transport, necessitating further chemical treatment for neutralization. Recently, Guo et al. [23] demonstrated that ion-exchange (IEX) resins have shown potential in improving the efficiency of TAN-removal from a low strength wastewater stream as a pre-treatment for BPMED. Although, it should be noted that the regeneration of IEX resins requires highly acidic solutions or a highly concentrated monovalent cation stream in the case of adsorbed divalent cations, for successful regeneration [24,25].

The process of TAN-removal and recovery with BPMED from residual streams faces high E_{TAN} for practical applications (18–25.2 MJ kgN^{-1}), non-controlled scaling, and NH_3 back-diffusion into the acid chamber [10,14,26]. Specifically, the E_{TAN} for TAN-removal from AD reject water has to be competitive to e.g. conventional denitrification (57 MJ kgN^{-1}) [27,28]. In order to utilise BPMED technology for TAN removal from real reject water, necessary modifications on its configuration needs to be applied to confront the already mentioned challenges. Although depending on the desired removal efficiency of TAN, a lower E_{TAN} of BPMED can be achieved than the previously reported 18.7 – 24.8 MJ kgN^{-1} [10,13,14]. With regards to NH_3 back-diffusion in the acid solution in a three-compartment BPMED, modifications on the configuration can be made into a two-compartment configuration (BPC) by neglecting the AEMs [13,29]. Thus, the transport of TAN is restricted to a single direction.

As shown in Fig. 2. when EDR is combined with BPC, the concentrate stream from EDR is already a factor 20 higher with regards to the electrical conductivity (EC). Furthermore, the reversed polarity allows the detachment of organic matter from the membranes and their simultaneous drainage from the loop. Once a higher concentration is achieved the concentrated of TAN solution is introduced directly into the two-compartment BPC. The activation of BPC enables a) the transport of only cations through the CEM into the base solution and b) the

dissociation of water which leads to the production of H^+ and OH^-. Thus, the concentrated solution by the EDR becomes an acidic solution once the buffer capacity is depleted. The process can be described by equation (1) where the production of CO_2 is the result of the depleted HCO_3^- that the EDR transported from the feed to the acid. The mechanism of buffer depletion is dependent on the transport rate of HCO_3^- by the EDR and the current density of BPC for the H^+ generation.

$$[HCO_3^-]_{EDR} + [H^+]_{BPC} \Leftrightarrow H_2CO_3 \Leftrightarrow CO_2 + H_2O \tag{1}$$
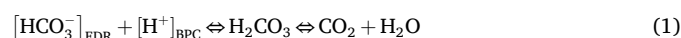
During transport of TAN into the base solution, other cations present in reject water such as K^+, Na^+, Ca^{2+} and Mg^{2+} are transported too. The alkaline environment in the base could result in the precipitation of Ca^{2+} and Mg^{2+} in the form of struvite, $CaCO_3$ and $Mg(OH)_2$. Precipitation of $CaCO_3$ has been shown to occur in previous studies [11,12,17,29] due to the transport of Ca^{2+} and CO_2 desorption through the CEM from the acid stream. To minimize inorganic scaling in the base chamber, monovalent selective cation-exchange membranes (MSCEMs) can be used in the feed to reduce the transport of divalent or multivalent cations [30–32]. Zhang et al. [33] demonstrated how ED with MSCEM improved the selectivity of monovalent cations over the divalent for the lowest applied current density of 4 mA·cm^{-2}. Thus, the performance of MSCEM in TAN selective removal in ED and BPMED from real AD reject water has not been investigated. The development of a selective electrodialysis reversal (SEDR) system with MSCEMs may offer a viable solution, providing a high concentration factor for TAN, while effectively lowering the concentration of divalent cations.

1.4. Research objective

This study suggests that the operational challenges can be mitigated by improving the configuration of the BPMED. The novel SEDR + BPC comes as the suggested configuration for TAN-removal from real sludge AD reject water with SEDR as the pre-treatment technology for BPC

while still having three chambers. The energy consumption for BPMED, EDR + BPC, and SEDR + BPC was compared on TAN-removal and recovery at three different load ratios (L_N). Furthermore, the contribution of MSCEMs on reducing scaling in the base chamber was assessed. The EDR + BPC and SEDR + BPC configurations were tested for reducing E_{TAN} and improving the potential NH_3 back-diffusion losses.

2. Materials and methods

2.1. Sludge reject water

A sludge AD reject water sample of 1000 L was collected from the WWTP Horstermeer, The Netherlands. The composition of this reject water (1 well-mixed grab sample) was as follows: Cl^- 701 mg·L^{-1}, PO_4^{3-} 123 mg·L^{-1}, SO_4^{2-}- 12 mg·L^{-1}, Na^+ 92 mg·L^{-1}, K^+ 582 mg·L^{-1}, Mg^{2+} 483 mg·L^{-1}, NH_4^+ 680–750 mg·L^{-1}, Ca^{2+} 58 mg·L^{-1}, HCO_3^- 3916 mg·L^{-1}, pH 7.8, TOC 135 mg·L^{-1}, TSS 192 mg·L^{-1}.

2.2. The setup

The set-up with electrochemical cells consisted of one ED cell and one BPMED cell, both designed and supplied by RedStack B.V. (Sneek, The Netherlands). The electrode chamber in both cells was equipped with an anode and a cathode. The electrodes had an active surface area of 10x10 cm^2 and consisted of Pt/Ir coating and metal-stretched TiO$_2$.

2.3. Electrodialysis stack

The ED cell was adjusted to operate as a conventional ED stack with two chambers of ten pairs of AEM and CEM membranes. Each pair contained a FKL-PK-130 CEM and a FAS-PET-130 AEM separated by 0.27 mm thickness wire mesh spacers, made of silicon/polyethylene sulfone, creating the diluate and the ED concentrate chamber. Thinner spacers than 0.5 mm were used to provide a thinner boundary layer of lower resistance [34]. In addition, two CEM end-membranes (CEEM) of F-10150-PTFE were placed at each side of the stack next to the electrodes as depicted in Fig. 2. The ED cell was later modified into a Selective ED (SED), by placing monovalent cation selective membranes (MCSM) (Astom, Japan) instead of standard CEM to achieve higher selectivity on NH_4^+ against divalent cations.

2.4. Bipolar membrane electrodialysis stacks

Two different configurations for the BPMED were tested. First, a BPMED configuration of ten membrane triplets was tested. The BPMED comprised of an acid chamber with acidic solution, a feed chamber with the feeding solution and the base chamber with base solution. The ion-exchange membranes were FAB-PK-130 as AEM, FBM-BPM as BPM and FKB-PK-130 as CEM. Also in this set-up, two CEEM were placed at each side of the stack adjacent to the electrodes.

A BPMED was modified into a BPC by excluding the acid chamber from the design. The acid and concentrate chambers were replaced by 1 single concentrate chamber that was connected to the ED-cell. The BPC contained ten membrane pairs, where each pair combined a BPM and a CEM. Each membrane pair consisted of an FBM-BPM and a FKB-PK-130. All the membranes were supplied by FUMATECH BWT GmbH (Baden-Württemberg, Germany).

2.5. Electrical design

The electric current in the ED cell was applied by Delta Elektronika power supply series SM800 with a range of 00.00–18.37 V and 00.00–50.00 A, while in the BPMED the Delta Elektronika power supply series SM1500 was applied with a range of 000.00–120.00 V and 00.00–13.00 A. A digital time relay designed to operate within a range of 20–240 V AC/DC (Crouzet, France) was connected to the power supply
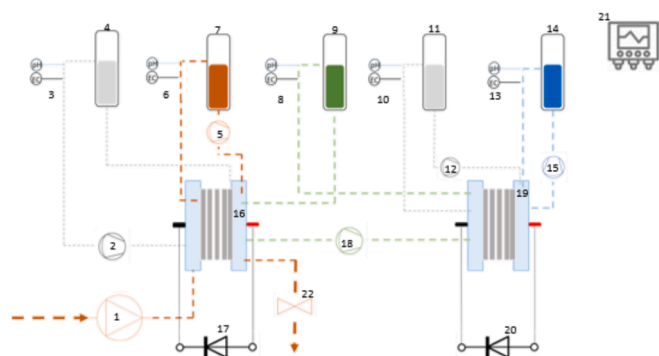
Fig. 3. The used experimental set-up comprised of an EDR/SEDR cell with feed and bleed (16), a BPC/BPMED cell (19), feeding pump (1), two power supplies (17, 20), recirculating diaphragm pumps (2, 5, 18, 12, 15), pH and EC sensors (3, 6, 8, 10, 13), recirculation vessels (4, 7, 9, 11, 14), a data logger (21) and a ("bleed" phase) draining valve (22).

of the ED in order to reverse the applied current in a timed cycle of 75:5 s (forward: reverse), thereby operating the ED with a reversal cycle as EDR. The solutions were circulated through the modules by calibrated Seaflo (Xiamen Doofar Outdoor Co., Ltd., China) diaphragm pumps at 20 L·h^{-1}. All the solutions contained initial volume of 2 L. The AD reject water was continuously fed into the diluate by a calibrated Grundfos (Bjerrinbro, Denmark) pump. The pH of the solutions was measured by Endress and Hauser calibrated pH probes, Memosens CPS11E in PVC in-lined armatures, connected to an 8-channel CM448 Liquiline transmitter. The electrical conductivities (EC) were measured by QC205X electrodes connected to P915-85 controller (QiS-Presence BV, Oosterhout, The Netherlands). The data for pH and EC were logged through a MultiCon CMC-99 data logger provided by SIMEX (Gdansk, Poland).

Water samples were taken every 1 h-interval during steady state of the desalination rate in the diluate according to the logged EC (Fig S.9). The samples were analysed with Ion Chromatography, Metrohm Compact IC Flex 930 with 883 cation system for the cations (Na^+, NH_4^+, K^+, Mg^{2+}, Ca^{2+}) and 818 anion system for the anions (Cl^-, SO_4^{2-}, PO_4^{3-}). Alkalinity was measured by SM Titrino 702 as mg/L of CaCO$_3$. Each sample presented in this study was a triplicate.

2.6. Experimental design

The 'feed and bleed' technique was applied at the diluate stream, as depicted in Fig. 3, to ensure a continuous supply of reject water into the ED cell. During the "feed" phase the pump supplied reject water into the diluate while the power supply of ED applied a forward current for 75 s. In contrast, during the "bleed" phase the diluate was drained from the system at an equivalent flow rate for 5 s while the power supply of ED applied a current in reversed direction. All experiments were terminated when the base solution had reached an EC of at least 3 mS·cm^{-1} and pH above 10. These targets are considered sufficient for potential vacuum stripping of NH_3 from the base solution via membrane contactor [7,35]. Tap-water was used as a starting solution in the base and acid that provided an initial EC of 0.5 mS·cm^{-1}. The aim was to simulate realistic conditions that could occur during an on-site initial phase. The experiments with EDR + BPC and SEDR + BPC were performed by initially operating the EDR and SEDR at the targeted L_N. Once the EC in the acid solution would reach the minimum of 20 mS·cm^{-1}, the activation of BPC was enabled. The electrode rinse solution (ERS) contained initially 0.15 M of Na$_2$SO$_4$ (in 1 L solution of demi-water).

2.7. Performance indicators

The removal efficiency was evaluated based on the efficiency of removing and transporting TAN from the feed stream. By relating the
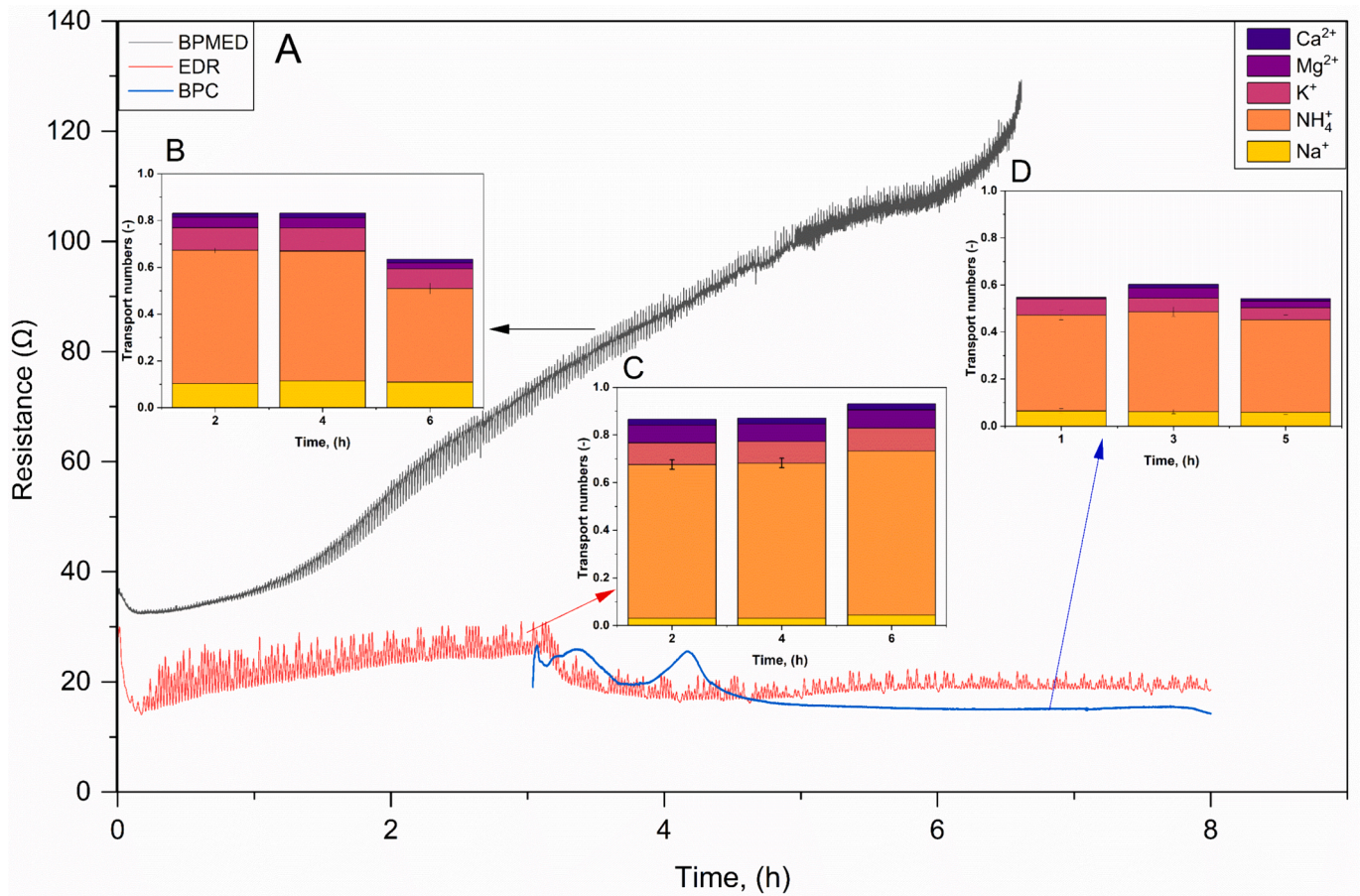
Fig. 4. A: Progression of electrical resistance (Ω) of the stacks measured as voltage-to-current ratio (V/I) for the BPMED and EDR + BPC configurations at an applied L_N of 1. The y-axis represents the resistance (values expressed in ohm (Ω)) for both configurations, while the x-axis denotes the operation time in hours. B: The transport numbers of cations in BPMED indicated with a black arrow. C: The transport numbers of cations in EDR indicated with a red arrow. D: The transport numbers of cations in BPC indicated with a blue arrow.

initial TAN concentration in the feed reject water ($C_{NH_4^+,feed}$) with the TAN concentration in the diluate stream ($C_{NH_4^+,diluate}$), the $\eta_{removal}$ as % was calculated for the time intervals (2, 4, 6, 8 h).

$$\eta_{removal} = \left(1 - \frac{C_{NH_4^+,diluate}}{C_{NH_4^+,feed}}\right) \bullet 100\% \qquad (2)$$

The recovery efficiency (%) was evaluated based on the efficiency of BPMED and BPC to transport TAN in the base solution from the overall removed TAN. Where $M_{NH_4^+,base}$ is the final mass in the base and the $M_{NH_4^+,removed}$ is total mass removed by BPMED, EDR, and SEDR.

$$\eta_{recovery} = \left(1 - \frac{M_{NH_4^+,base}}{M_{NH_4^+,removed}}\right) \bullet 100\% \qquad (3)$$

The energy consumption for transported TAN (E_{TAN}) was calculated for each module independently. The E_{TAN} in MJ kgN^{-1} was calculated for EDR, SEDR, BPC, and BPMED.

$$E_{TAN} = \frac{\sum_{t=0}^{t}(U_{\Delta t} \bullet I_{\Delta t} \bullet \Delta t)}{\Delta M_{NH_4^+}} \bullet 10^{-6} \qquad (4)$$

where $U_{\Delta t}$ = average electric potential (in V) over a time interval Δt between two sampling points, $I_{\Delta t}$ = average applied current during the time interval (in A), $\Delta M_{NH_4^+}$ = the difference in mass (g) between the total TAN that entered the stack and the total residual TAN in the diluate.

The transport number of cations was calculated based on the difference in molar mass between the influent and the effluent over the total produced current for a specific time interval.

$$t_i = \frac{z \bullet F \bullet \Delta M_i}{N \bullet I \bullet \Delta t} \qquad (5)$$

where z is the ion valance, F the Faraday constant, ΔM the molarity difference between the solutions of two chambers across the CEM, N the number of pairs or triplets, I the applied current density (A·m^{-2}) and Δt the time interval (s).

The resistance (R) was calculated after dividing the average obtained voltage (V) with the average applied electrical current (A).

$$R = \frac{V}{I} \qquad (6)$$

The concept of load ratio (L_N) was employed to characterize the operational conditions equally for every configuration based on varying TAN concentration in the feed. The applied load ratio was calculated based on the formula that was first derived by Rodriguez Arredondo et al. [36]

$$L_N = \frac{I_{applied}}{C_{TAN,inflow} \bullet Q_{in} \bullet \frac{F}{A_m}} \qquad (7)$$

where $I_{applied}$ is the applied current density (A·m^{-2}), $C_{TAN, inflow}$, is the molar concentration of TAN in the feeding reject water (mol·m^{-3}), Q_{in} the reject water flow rate (m^3 ·s^{-1}), F the Faraday constant (96485C·mol^{-1}) and A_m the surface area of the CEM (0.01 m^2).

The molar ratio in the diluate was calculated by the moles of TAN
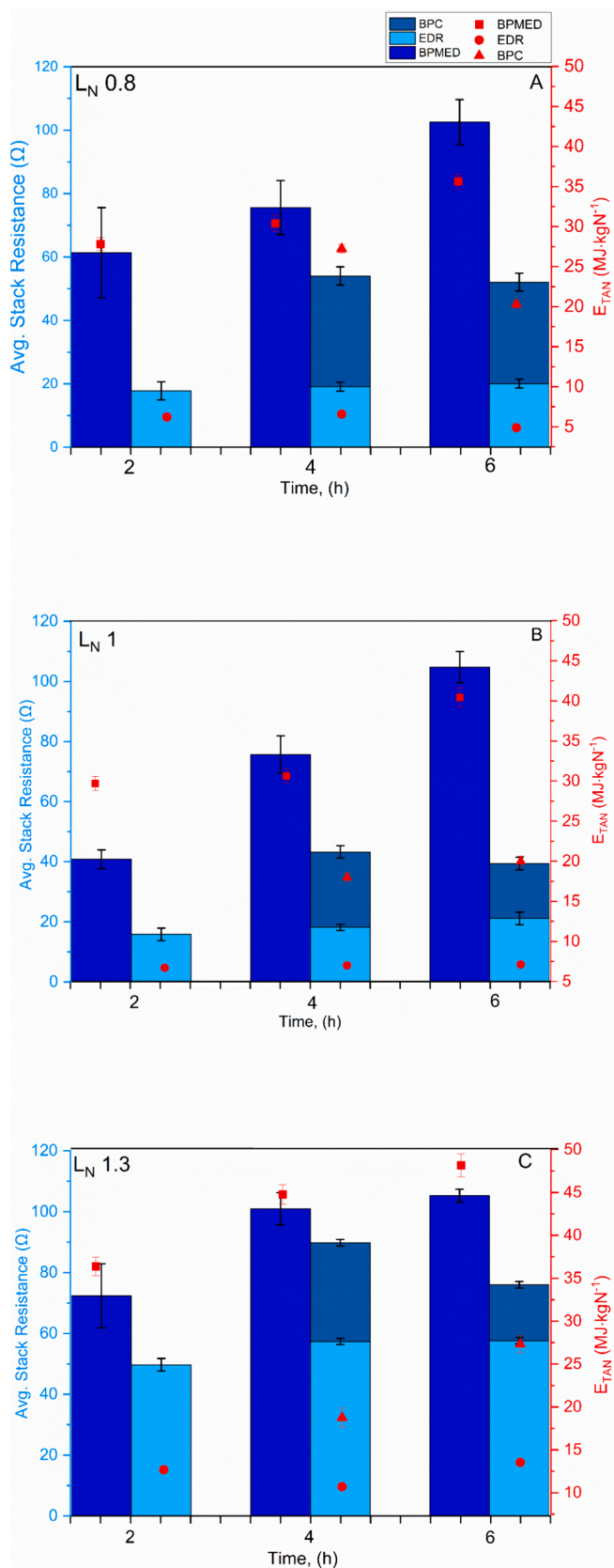
Fig. 5. The resistance and energy consumption of BPMED and EDR + BPC for all the applied load ratios. The average resistance of the stacks is indicated on the left y-axis with shades of blue colour by the stacked columns. On the right y-axis is indicated the energy consumption with shapes of red colour by the scatter diagram. Graph A: L_N 0.8, B: L_N 1 and C: L_N 1.3.

over the summed moles of Mg^{2+} and Ca^{2+}.

$$Molar\,ratio = \frac{n_{TAN,}}{n_{Mg^{2+}} + n_{Ca^{2+}}} \tag{8}$$

3. Results and discussion

The tested configurations, namely BPMED, EDR + BPC, and SEDR + BPC, were subjected to the same operational conditions and categorized based on the applied load ratio (L_N). Each experiment was duplicated and all standard deviations presented are less than 6 %.

3.1. EDR + BPC configuration: A superior approach for resistance reduction compared to stand-alone BPMED

In Fig. 4 the BPMED configuration exhibited a gradual increase in cell resistance until the target in electrical conductivity of 3 mS cm^{-1} was reached in the base solution, corresponding with a resistance of 130 Ω. In contrast, the EDR + BPC configuration maintained a consistently low cell resistance of 21 Ω throughout the process until achieving the desired 3 mS cm^{-1}. Potential causes for the progressive increase in resistance of the BPMED cell were scaling on the CEM and organic fouling on the surface of the AEM membrane. Inspection of the cell during disassembly of BPMED showed that scaling was prevalent on the CEM and the spacers in the base solution. Previous studies have reported the disruption in the continuous process of ED due to inorganic scaling [12]. Furthermore, the accumulation of organic compounds could also cause an increase in membrane resistance especially on the surface of the AEM [37,38]. In contrast to the BPMED, the EDR + BPC configuration exhibited a stable resistance profile. BPMED faced a drop in transport efficiency during the continuous operation, which was attributed to scaling (Fig S5) in the base solution and potential attachment of organics on the AEM. As a result, the desalination rate of the dilutae for BPMED during L_N1 and 1.3 started to decrease as seen in Fig S9 (B and C). Contrariwise, the transport numbers especially for TAN, did not face a proportional drop in EDR + BPC compared to BPMED after 4 h. In the EDR module, the transport efficiency for TAN was improved after the activation of BPC, while it remained almost stable in the BPC. The lower transport numbers found for BPC compared to BPMED were attributed to the competitive transport of H$^+$ and the re-transport of back-diffused TAN. It was hypothesized that the lower resistance in both modules of the EDR + BPC configuration was attributable to the increased electrochemical gradient enabled by EDR and the accumulation of H$^+$ in the solution of acid-chamber, which provided an increased EC. Thus, providing higher concentrations of TAN by the EDR resulted in higher transport of TAN [39], while H$^+$ production in the BPC resulted in a voltage decrease in the EDR.

Fig. 5 shows that eventually the average stack resistance for BPMED was higher than for the combined EDR + BPC for every applied L_N. Consequently, the fouling mechanisms combined with the lower concentration gradient that BPMED faced contributed to a much higher energy consumption, while the EDR + BPC achieved a more stabilised and lower trajectory.

3.2. Higher concentration gradient by EDR + BPC resulted in increased recovery of TAN

During the incorporation of the BPC, an initial drop in EC of the acid was observed due to the transport of cations to the base (Fig. 6(A)). This drop potentially occurred as a result of depleted buffer capacity in the acid solution, due to reactions with the accumulating H$^+$. Since part of the transported charge is substituted by free H$^+$, which was continuously produced by the BPM, the HCO$_3^-$ related buffer capacity of the reject water depleted [40] and CO$_2$ was generated as described by equation (1). Results depicted in Fig. 6(B) showed that the higher EC gradient generated by the EDR resulted in a faster and steeper EC gradient in the
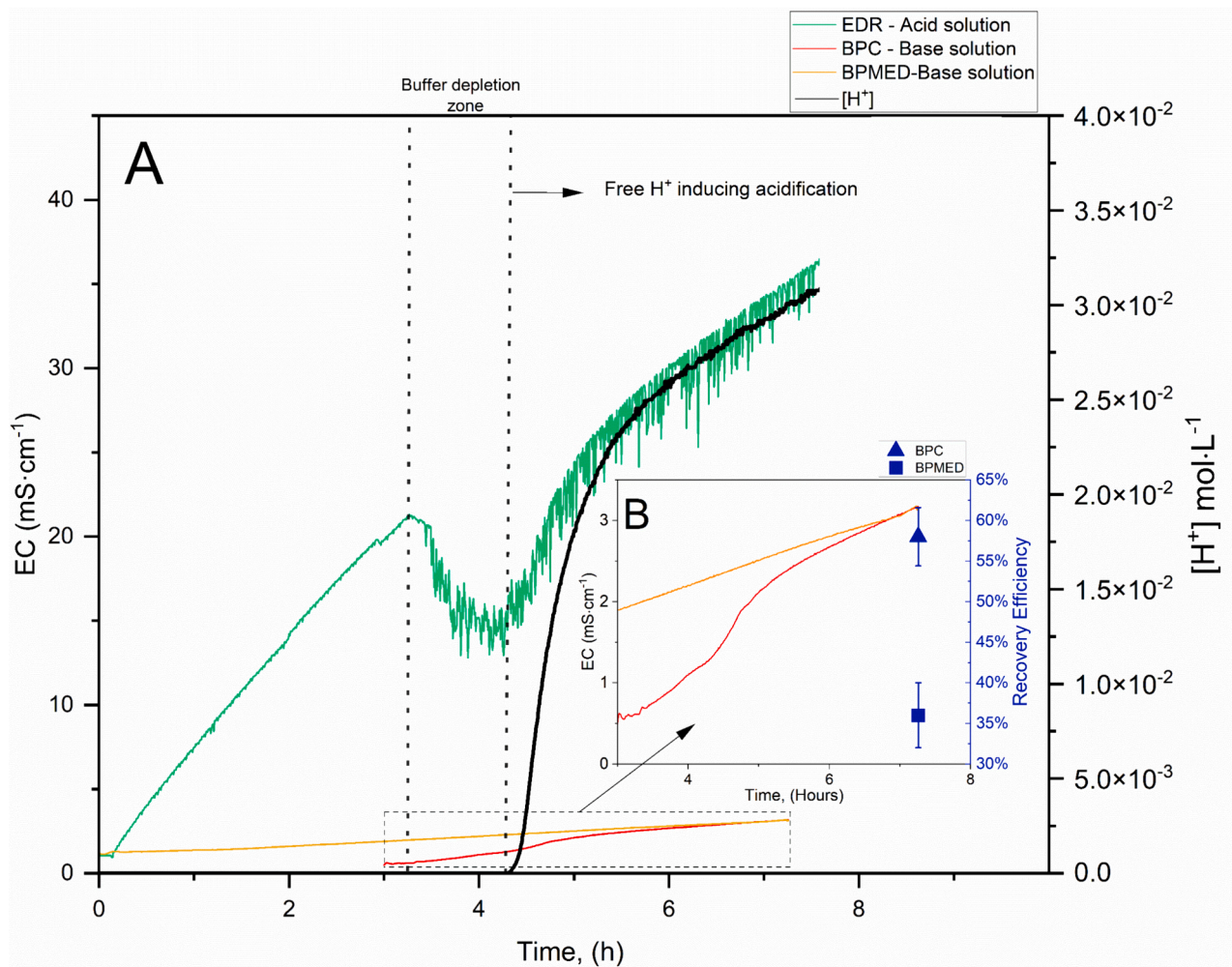
Fig. 6. The concentration gradient expressed as electrical conductivity and the recovery efficiency for EDR + BPC and BPMED, applying an L_N of 1. A: EC in mS cm^{-1} for acid and base. The left y-axis indicates the EC of the acid concentrate solution and the right y-axis depicts the free H$^+$ as molarity. The x-axis corresponds to the time in hours. The produced CO$_2$ caused the oscillations on the EC sensors which is observed after the activation of the BPC at 3 h once the target of 20 mS·cm^{-1} be the EDR in the acid was reached. B: The left y-axis indicates the EC in mS cm^{-1} and the right y-axis the recovery efficiency in (%) for BPMED and BPC in the base solution. The error bars of the recovery efficiency values correspond to minimum and maximum values.

base concentrate of the BPC compared to the BPMED.

The generation of H$^+$ ions and the subsequent acidification of the concentrate provided an additional driving force for the observed higher electrochemical gradient. While the presence of H$^+$ ions in the concentrate could potentially compete with the transport of TAN through the CEM of the BPC, the acidified conditions effectively minimised precipitation but also NH$_3$ back-diffusion. In fact, the EDR + BPC configuration enabled the transport of TAN at one single direction towards the base. The potentially back-diffused NH$_3$ gets ionised to NH$_4^+$ into the acid, and is being re-transported to the base. As a result, the EDR + BPC achieved a higher recovery of TAN in the base compared to BPMED as a result of reduced back-diffused NH$_3$ (Fig. 6(B)).

Although the effect of free H$^+$ provided a reducing trajectory in resistance, future research should investigate the effect of accumulating acid at the feed-side of the BPC. Due to accumulating acid, the EDR transported HCO$_3^-$ was transformed into CO$_2$. The produced CO$_2$ could potentially desorb into the base, causing CaCO$_3$ precipitation. Thus, it is necessary to investigate whether acidified conditions, are indeed beneficial for the EDR + BPC configuration.

3.3. Monovalent selective membranes improved the transport selectivity for TAN

Although the EDR + BPC configuration provided an improvement on the TAN removal and recovery from real reject water, high transport of divalent cations and scaling formation was still prevalent for almost all the experiments. Therefore, to mitigate the phenomena of scaling and improve the transport of TAN the MSCEMs were employed in EDR + BPC configuration, forming an SEDR + BPC. To illustrate the effects of this alteration, Fig. 7 shows the cation molar ratio (n_{TAN}:n_{Mg}^{2+}) for the diluate solution in both EDR + BPC and SEDR + BPC configurations and the total TAN-flux.

The SEDR + BPC configuration indeed transported more TAN and less divalent cations into the base solution compared to EDR + BPC, while the n_{TAN}:n_{Mg}^{2+} of the diluate was lower for SEDR + BPC than that of EDR + BPC for all applied L_N. The lower n_{TAN}:n_{Mg}^{2+} values evidenced a higher selectivity for monovalent cations of the MSCEMs, which also resulted in a higher TAN-flux achieved by SEDR + BPC. Furthermore, the selectivity of the transported TAN when expressed by transport numbers showed that indeed a higher share of transported charge was achieved by the MSCEMs (Fig. S2).
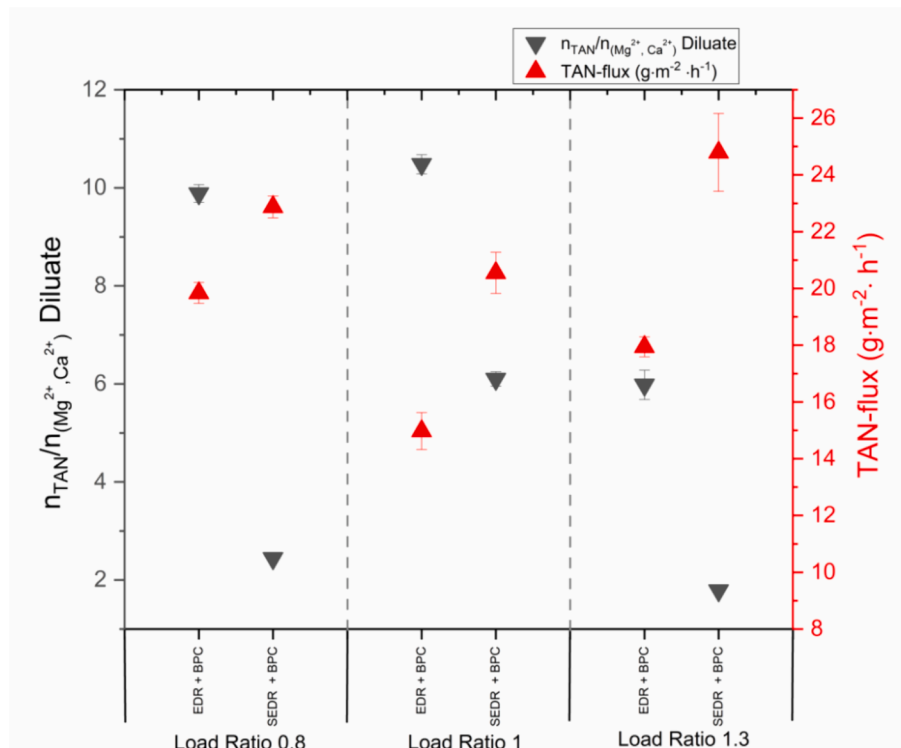
Fig. 7. On the left y-axis, the molar ratio of TAN to cations (Mg^{2+} and Ca^{2+}) in the diluate is represented as $n_{TAN}:n_{cations}$. The right y-axis displays the average TAN flux in grams per square meter per hour ($g \cdot m^{-2} \cdot h^{-1}$). The values are presented for the EDR + BPC and SEDR + BPC configurations across various load ratios indicated on the x-axis.
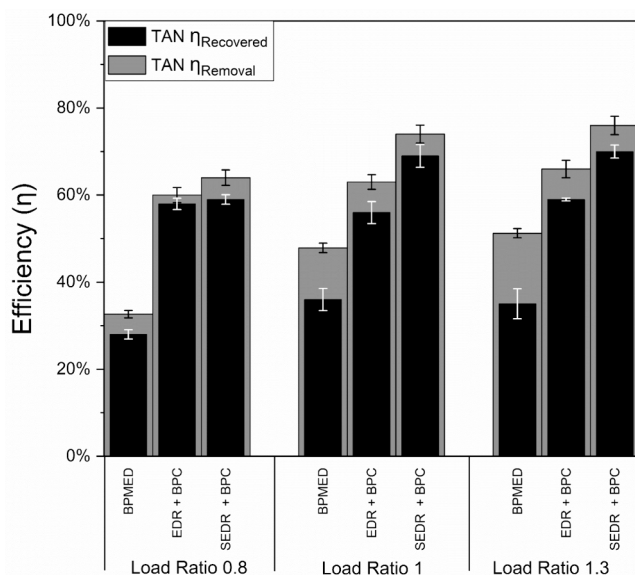
Fig. 8. The η of TAN in % from reject water achieved by BPMED, EDR + BPC and, SEDR + BPC at L_N 0.8, 1 and 1.3.

3.4. Removal efficiency: SEDR + BPC shows higher $\eta_{removal}$ of TAN compared to conventional EDR + BPC and BPMED

Fig. 8 shows the obtained $\eta_{removal}$ for L_N 0.8, 1, and 1.3 in all three configurations. The SEDR + BPC configuration had a distinct higher $\eta_{removal}$ compared to the BPMED and EDR + BPC, especially at L_N 1 and 1.3. Specifically, the SEDR + BPC achieved the highest $\eta_{removal}$ reaching 65 %, 75 %, and 78 %, at an applied L_N of 0.8, 1, and 1.3, respectively. The BPMED performed poorly compared to SEDR + BPC with achieved

$\eta_{removal}$ of only 33 %, 48 %, and 52 % at an L_N 0.8, 1, and 1.3, respectively. These results clearly evidenced the positive contribution of MSCEMs in enhancing TAN-removal at all applied L_N values. In line with the findings of Rodrigues et al.[11,12], a correlation between L_N and $\eta_{removal}$ was observed, with a substantial increase, when transitioning from L_N 0.8 to 1, and only marginal improvement from L_N 1 to 1.3.

Regarding $\eta_{recovery}$, BPMED consistently yielded the lowest recovery rates among all the configurations, applying the different L_N. The observed poor performance using BPMED can be attributed to the combination of a lower concentration gradient of TAN in the feed and NH_3 back-diffusion in the acid, resulting in reduced TAN removal and recovery, as well as higher losses of TAN. The losses of TAN are depicted in Fig. 8, represented by the gap between removal and recovery. Notably, these losses were minimized when utilizing EDR + BPC and especially, SEDR + BPC. The highest $\eta_{recovery}$ was observed at an L_N of 1.3 for SEDR + BPC, reaching 69 %. In general, SEDR + BPC consistently achieved higher recovery rates compared to both BPMED and EDR + BPC especially at L_N 1 and 1.3, potentially owing to the enhanced N-fluxes facilitated by the MSCEMs.

It is worth noting that EDR + BPC demonstrated superior $\eta_{removal}$ performance compared to BPMED, despite similar operational conditions. Based on the present results, this is attributed to the back-diffusion of TAN using BPMED, where TAN migrates from the base to the diluate side, enriching the diluate with TAN. Furthermore, the presence of inorganic scaling on the surface of the CEM in BPMED, as depicted in Fig. 4, likely hindered the transport of TAN through the membrane, thereby influencing the overall $\eta_{removal}$.

3.5. Energy consumption for removal and recovery: Lowest E_{TAN} at L_N 0.8

Evaluating all used configurations, the lowest E_{TAN} of 4.4 $MJ \cdot kgN^{-1}$ for TAN-removal at an L_N of 0.8 was achieved by SEDR + BPC (Fig. 9). Similarly SEDR + BPC achieved the lowest E_{TAN} of 13 $MJ \cdot kgN^{-1}$ for N recovery, but only for the case when an L_N of 0.8 was applied. Since
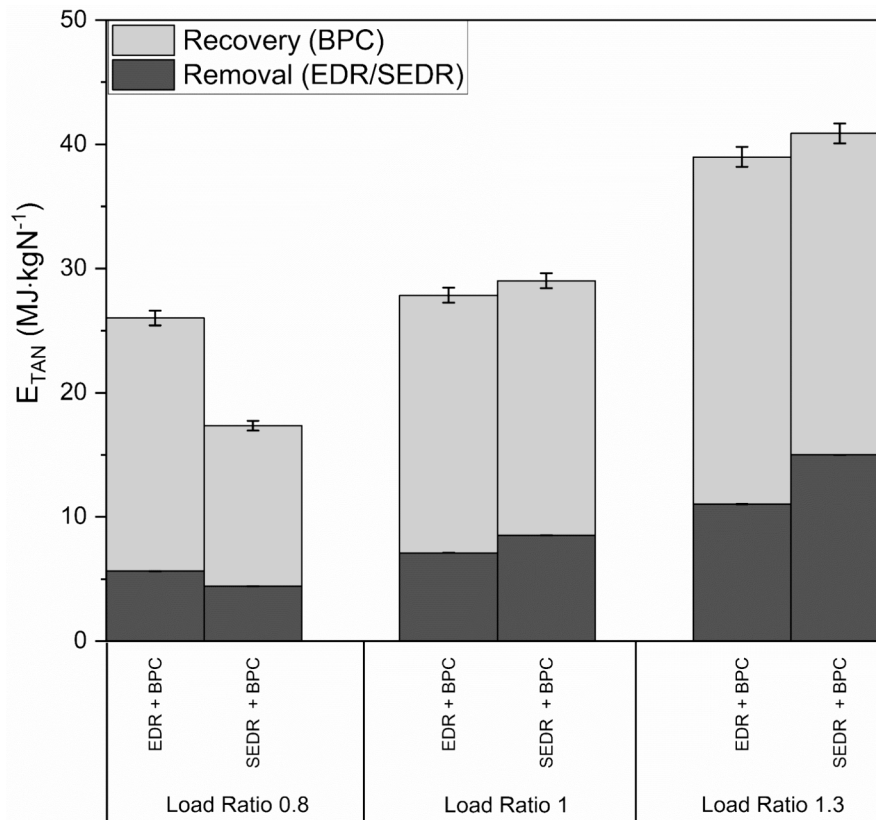
Fig. 9. E_{TAN} in MJ·kgN^{-1} for removal and recovery by EDR + BPC and SEDR + BPC at an L_N of 0.8, 1 and, 1.3.

scaling was minimum at L_N 0.8 and considering the low achieved molar ratio in the diluate (Fig. 7), the performance of the BPC module using the SEDR + BPC configuration was optimal. For the case of L_N 1 and 1.3, the SEDR + BPC had higher E_{TAN} which was likely attributable to the higher resistance of the MSCEMs compared to standard CEMs.

For the EDR + BPC configuration, the transition from L_N 0.8 to 1.3 caused E_{TAN} to increase by a factor of 2. This pattern was even more pronounced in the case of SEDR + BPC, where an increase of L_N from 0.8 to 1.3 resulted in an increase of E_{TAN} by a factor of 3.4. In contrast, the corresponding improvements in $\eta_{removal}$ (Fig. 8) were comparatively minor, marked by increase factors of only 1.2 and 1.1, respectively. Thus, there was minimum gain in $\eta_{removal}$ with increasing L_N, while E_{TAN} substantially increased. In comparison to other studies, Ward et al. [17] achieved 23 % $\eta_{removal}$ at an E_{TAN} of 13 MJ·kgN^{-1} in an ED pilot plant, using AD reject water of a municipal WWTP. Similarly, in a BPC pilot plant study by Ferrari et al. [13], the BPC achieved 58.1 % $\eta_{removal}$ at an E_{TAN} of 42.4 MJ·kgN^{-1}, using similar feed water. However, van Linden et al. [14] demonstrated that BPMED, using a synthetic NH$_4$HCO$_3$ feed water, achieved a lower $\eta_{recovery}$ of 49 %, due to NH$_3$ back-diffusion losses at an E_{TAN} of 18 MJ·kgN^{-1} for removal. Finally, future research should investigate the impact of organic fouling on the AEM of the SEDR especially during much longer operations.

4. Conclusions

Comparing the BPMED with the novel SEDR + BPC configuration, results evidenced that the latter represents a superior alternative for resistance reduction and overall transport efficiency. The SEDR + BPC configuration improved the overall performance tackling more effectively the challenges of a low concentration gradient, NH$_3$ back-diffusion, inorganic scaling, and high E_{TAN}. Thus, SEDR + BPC is regarded a promising approach for improving the performance of pro-longed continuous operation scenarios during the treatment of complex

feed waters, such as municipal sludge reject water. Considering the treatment of challenging streams, such as real sludge reject water. The findings conclude the following:

- BPMED as a stand-alone approach for removal of TAN directly from real AD reject water faced challenges of low concentration gradient, NH$_3$ back-diffusion, scaling and high E_{TAN}. The BPMED showed faster progressing stack resistance with highest E_{TAN} of 31–47 MJ ·kgN^{-1}.
- The generation of high concentration gradient by the EDR + BPC in combination with the self-cleaning mechanism showed a more sta-bilised transport efficiency of TAN and better regulated stack resis-tance than the BPMED configuration across time.
- The EDR + BPC showed a higher $\eta_{recovery}$ of TAN compared to BPMED enabling the transport of TAN at one single direction towards the base minimising back-diffusion of NH$_3$.
- The transported HCO$_3^-$ by the EDR into the acid resulted in the production of CO$_2$ after reacting with the generated H$^+$ by the BPC. During acidification, CO$_2$ could have potentially desorbed through the CEM reacting with the transported Ca^{2+} and cause precipitation of CaCO$_3$.
- A further improvement of the EDR + BPC was achieved by the replacement of standard CEM with MSCEMs. The resulted SEDR + BPC configuration improved the transport of TAN over the divalent cations such as Ca^{2+} and Mg^{2+} and achieved higher fluxes of TAN to the acid.
- The highest $\eta_{removal}$ was at L_N 1.3 for SEDR + BPC at 78 %, and the highest $\eta_{recovery}$ at 69 %, minimising the losses between removed and recovered TAN.
- SEDR + BPC achieved the lowest E_{TAN} among all the configurations with 4.4 MJ·kgN^{-1} for TAN-removal and 13 MJ kgN^{-1} for recovery during L_N of 0.8.

CRediT authorship contribution statement

Iosif Kaniadakis: Writing – review & editing, Writing – original draft, Visualization, Methodology, Investigation, Formal analysis, Data curation, Conceptualization. **Jules B. van Lier:** . **Henri Spanjers:** Writing – review & editing, Validation, Supervision, Project administration.

Declaration of competing interest

The authors declare the following financial interests/personal relationships which may be considered as potential competing interests: Iosif Kaniadakis reports financial support was provided by Delft University of Technology. Iosif Kaniadakis reports a relationship with Delft University of Technology that includes: employment. If there are other authors, they declare that they have no known competing financial interests or personal relationships that could have appeared to influence the work reported in this paper.

Data availability

Data will be made available on request.

Appendix A. Supplementary data

Supplementary data to this article can be found online at https://doi.org/10.1016/j.cej.2024.152613.

References

[1] Q. Zhang, F. Ren, F. Li, G. Chen, G. Yang, J. Wang, K. Du, S. Liu, Z. Li, Ammonia nitrogen sources and pollution along soil profiles in an in-situ leaching rare earth ore, Environ. Pollut. 267 (2020) 115449, https://doi.org/10.1016/J.ENVPOL.2020.115449.

[2] A.T.M.A. Choudhury, I.R. Kennedy, Nitrogen fertilizer losses from rice soils and control of environmental pollution problems, Commun. Soil Sci. Plant Anal. 36 (2005) 1625–1639, https://doi.org/10.1081/CSS-200059104.

[3] Š. Höfferle, G.W. Nicol, L. Pal, J. Hacin, J.I. Prosser, I. Mandić-Mulec, Ammonium supply rate influences archaeal and bacterial ammonia oxidizers in a wetland soil vertical profile, FEMS Microbiol. Ecol. 74 (2010) 302–315, https://doi.org/10.1111/j.1574-6941.2010.00961.x.

[4] J.W. Erisman, J. Galloway, S. Seitzinger, A. Bleeker, K. Butterbach-Bahl, Reactive nitrogen in the environment and its effect on climate change, Curr. Opin. Environ. Sustain. 3 (2011) 281–290, https://doi.org/10.1016/J.COSUST.2011.08.012.

[5] Z. Deng, N. van Linden, E. Guillen, H. Spanjers, J.B. van Lier, Recovery and applications of ammoniacal nitrogen from nitrogen-loaded residual streams: A review, J. Environ. Manage. 295 (2021) 113096, https://doi.org/10.1016/J.JENVMAN.2021.113096.

[6] N. van Linden, H. Spanjers, J.B. van Lier, Fuelling a solid oxide fuel cell with ammonia recovered from water by vacuum membrane stripping, Chem. Eng. J. 428 (2022) 131081, https://doi.org/10.1016/J.CEJ.2021.131081.

[7] N. van Linden, Y. Wang, E. Sudhölter, H. Spanjers, J.B. van Lier, Selectivity of vacuum ammonia stripping using porous gas-permeable and dense pervaporation membranes under various hydraulic conditions and feed water compositions, J Memb Sci 642 (2022) 120005, https://doi.org/10.1016/J.MEMSCI.2021.120005.

[8] L. Shi, S. Xie, Z. Hu, G. Wu, L. Morrison, P. Croot, H. Hu, X. Zhan, Nutrient recovery from pig manure digestate using electrodialysis reversal: Membrane fouling and feasibility of long-term operation, J Memb Sci 573 (2019), https://doi.org/10.1016/j.memsci.2018.12.037.

[9] Y. Li, S. Shi, H. Cao, X. Wu, Z. Zhao, L. Wang, Bipolar membrane electrodialysis for generation of hydrochloric acid and ammonia from simulated ammonium chloride wastewater, Water Res. 89 (2016), https://doi.org/10.1016/j.watres.2015.11.038.

[10] Y. Li, R. Wang, S. Shi, H. Cao, N.Y. Yip, S. Lin, Bipolar Membrane Electrodialysis for Ammonia Recovery from Synthetic Urine: Experiments, Modeling, and Performance Analysis, Environ. Sci. Tech. 55 (2021) 14886–14896, https://doi.org/10.1021/acs.est.1c05316.

[11] M. Rodrigues, T. Sleutels, P. Kuntke, D. Hoekstra, A. ter Heijne, C.J.N. Buisman, H.V.M. Hamelers, Exploiting Donnan Dialysis to enhance ammonia recovery in an electrochemical system, Chem. Eng. J. 395 (2020) 125143, https://doi.org/10.1016/j.cej.2020.125143.

[12] M. Rodrigues, A. Paradkar, T. Sleutels, A. ter Heijne, C.J.N. Buisman, H.V.M. Hamelers, P. Kuntke, Donnan Dialysis for scaling mitigation during electrochemical ammonium recovery from complex wastewater, Water Res. 201 (2021) 117260, https://doi.org/10.1016/j.watres.2021.117260.

[13] F. Ferrari, M. Pijuan, S. Molenaar, N. Duinslaeger, T. Sleutels, P. Kuntke, J. Radjenovic, Ammonia recovery from anaerobic digester centrate using onsite pilot scale bipolar membrane electrodialysis coupled to membrane stripping, Water Res. 218 (2022) 118504, https://doi.org/10.1016/J.WATRES.2022.118504.

[14] N. van Linden, G.L. Bandinu, D.A. Vermaas, H. Spanjers, J.B. van Lier, Bipolar membrane electrodialysis for energetically competitive ammonium removal and dissolved ammonia production, J. Clean. Prod. 259 (2020) 120788, https://doi.org/10.1016/J.JCLEPRO.2020.120788.

[15] H. Strathmann, Electrodialysis, a mature technology with a multitude of new applications, Desalination 264 (2010) 268–288, https://doi.org/10.1016/J.DESAL.2010.04.069.

[16] N. van Linden, H. Spanjers, J.B. van Lier, Application of dynamic current density for increased concentration factors and reduced energy consumption for concentrating ammonium by electrodialysis, Water Res. 163 (2019) 114856, https://doi.org/10.1016/j.watres.2019.114856.

[17] A.J. Ward, K. Arola, E. Thompson Brewster, C.M. Mehta, D.J. Batstone, Nutrient recovery from wastewater through pilot scale electrodialysis, Water Res 135 (2018) 57–65. https://doi.org/10.1016/J.WATRES.2018.02.021.

[18] M. Mondor, L. Masse, D. Ippersiel, F. Lamarche, D.I. Massé, Use of electrodialysis and reverse osmosis for the recovery and concentration of ammonia from swine manure, Bioresour. Technol. 99 (2008) 7363–7368, https://doi.org/10.1016/J.BIORTECH.2006.12.039.

[19] Z. Zhao, S. Shi, H. Cao, Y. Li, B. Van der Bruggen, Comparative studies on fouling of homogeneous anion exchange membranes by different structured organics in electrodialysis, J. Environ. Sci. 77 (2019) 218–228, https://doi.org/10.1016/j.jes.2018.07.018.

[20] Y. Zhang, E. Desmidt, A. Van Looveren, L. Pinoy, B. Meesschaert, B. Van Der Bruggen, Phosphate separation and recovery from wastewater by novel electrodialysis, Environ. Sci. Tech. 47 (2013) 5888–5895, https://doi.org/10.1021/es4004476.

[21] C.M. Mehta, W.O. Khunjar, V. Nguyen, S. Tait, D.J. Batstone, Technologies to recover nutrients from waste streams: A critical review, Crit. Rev. Environ. Sci. Technol. 45 (2015) 385–427, https://doi.org/10.1080/10643389.2013.866621.

[22] A. Zarebska, D. Romero Nieto, K.V. Christensen, L. Fjerbæk Søtoft, B. Norddahl, Ammonium fertilizers production from manure: A critical review, Crit. Rev. Environ. Sci. Technol. 45 (2015) 1469–1521, https://doi.org/10.1080/10643389.2014.955630.

[23] X. Guo, J. Chen, X. Wang, Y. Li, Y. Liu, B. Jiang, Sustainable ammonia recovery from low strength wastewater by the integrated ion exchange and bipolar membrane electrodialysis with membrane contactor system, Sep. Purif. Technol. 305 (2023) 122429, https://doi.org/10.1016/j.seppur.2022.122429.

[24] M. Vanoppen, G. Stoffels, C. Demuytere, W. Bleyaert, A.R.D. Verliefde, Increasing RO efficiency by chemical-free ion-exchange and Donnan dialysis: Principles and practical implications, Water Res. 80 (2015) 59–70, https://doi.org/10.1016/J.WATRES.2015.04.030.

[25] T. Rijnaarts, N.T. Shenkute, J.A. Wood, W.M. De Vos, K. Nijmeijer, Divalent Cation Removal by Donnan Dialysis for Improved Reverse Electrodialysis, ACS Sustain. Chem. Eng. 6 (2018) 7035–7041, https://doi.org/10.1021/acssuschemeng.8b00879.

[26] E. Gain, S. Laborie, P. Viers, M. Rakib, G. Durand, D. Hartmann, Ammonium nitrate wastewater treatment by coupled membrane electrolysis and electrodialysis, (2002) 969–975. https://doi.org/https://doi.org/10.1023/A:1020908702406.

[27] S. Lackner, E.M. Gilbert, S.E. Vlaeminck, A. Joss, H. Horn, M.C.M. van Loosdrecht, Full-scale partial nitritation/anammox experiences – An application survey, Water Res. 55 (2014) 292–303, https://doi.org/10.1016/j.watres.2014.02.032.

[28] T. Schaubroeck, H. De Clippeleir, N. Weissenbacher, J. Dewulf, P. Boeckx, S.E. Vlaeminck, B. Wett, Environmental sustainability of an energy self-sufficient sewage treatment plant: Improvements through DEMON and co-digestion, Water Res. 74 (2015) 166–179, https://doi.org/10.1016/j.watres.2015.02.013.

[29] M. Rodrigues, S. Molenaar, J. Barbosa, T. Sleutels, H.V.M. Hamelers, C.J.N. Buisman, P. Kuntke, Effluent pH correlates with electrochemical nitrogen recovery efficiency at pilot scale operation, Sep. Purif. Technol. 306 (2023) 122602, https://doi.org/10.1016/J.SEPPUR.2022.122602.

[30] J. Lambert, M. Avila-Rodriguez, G. Durand, M. Rakib, Separation of sodium ions from trivalent chromium by electrodialysis using monovalent cation selective membranes, J Memb Sci 280 (2006) 219–225, https://doi.org/10.1016/J.MEMSCI.2006.01.021.

[31] Z.-L. Ye, K. Ghyselbrecht, A. Monballiu, T. Rottiers, B. Sansen, L. Pinoy, B. Meesschaert, Fractionating magnesium ion from seawater for struvite recovery using electrodialysis with monovalent selective membranes, Chemosphere 210 (2018) 867–876, https://doi.org/10.1016/j.chemosphere.2018.07.078.

[32] B. Cohen, N. Lazarovitch, J. Gilron, Upgrading groundwater for irrigation using monovalent selective electrodialysis, Desalination 431 (2018) 126–139, https://doi.org/10.1016/j.desal.2017.10.030.

[33] W. Zhang, M. Miao, J. Pan, A. Sotto, J. Shen, C. Gao, B. Van der Bruggen, Separation of divalent ions from seawater concentrate to enhance the purity of coarse salt by electrodialysis with monovalent-selective membranes, Desalination 411 (2017) 28–37, https://doi.org/10.1016/J.DESAL.2017.02.008.

[34] D.A. Vermaas, M. Saakes, K. Nijmeijer, Enhanced mixing in the diffusive boundary layer for energy generation in reverse electrodialysis, J Memb Sci 453 (2014) 312–319, https://doi.org/10.1016/J.MEMSCI.2013.11.005.

[35] M.S. EL-Bourawi, M. Khayet, R. Ma, Z. Ding, Z. Li, X. Zhang, Application of vacuum membrane distillation for ammonia removal, J Memb Sci 301 (2007) 200–209. https://doi.org/10.1016/j.memsci.2007.06.021.

[36] M. Rodríguez Arredondo, P. Kuntke, A. ter Heijne, C.J. Buisman, The concept of load ratio applied to bioelectrochemical systems for ammonia recovery, Journal of Chemical Technology & Biotechnology 94 (2019) 2055–2061. https://doi.org/10.1002/jctb.5992.

[37] N. Tanaka, M. Nagase, M. Higa, Organic fouling behavior of commercially available hydrocarbon-based anion-exchange membranes by various organic-fouling substances, Desalination 296 (2012) 81–86, https://doi.org/10.1016/J.DESAL.2012.04.010.

[38] W. Xiang, J. Yao, S. Velizarov, L. Han, Unravelling the fouling behavior of anion-exchange membrane (AEM) by organic solute of varying characteristics, J Memb Sci 662 (2022) 120986, https://doi.org/10.1016/J.MEMSCI.2022.120986.

[39] A.M. Hulme, C.J. Davey, S. Tyrrel, M. Pidou, E.J. McAdam, Transitioning from electrodialysis to reverse electrodialysis stack design for energy generation from high concentration salinity gradients, Energy Convers Manag 244 (2021) 114493, https://doi.org/10.1016/j.enconman.2021.114493.

[40] S. Wyffels, P. Boeckx, K. Pynaert, D. Zhang, O. Van Cleemput, G. Chen, W. Verstraete, Nitrogen removal from sludge reject water by a two-stage oxygen-limited autotrophic nitrification denitrification process, Water Sci. Technol. 49 (2004) 57–64, https://doi.org/10.2166/wst.2004.0737.